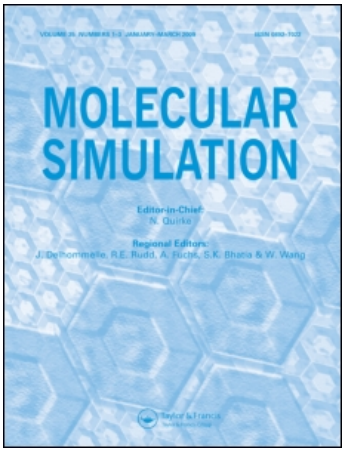

Molecular Simulation
Publication details, including instructions for authors and subscription information:
http://www.informaworld.com/smpp/title~content=t713644482

Electron states of semiconductor quantum ring with geometry and size variations

I. Filikhin[a]; E. Deyneka[b]; H. Melikyan[a]; B. Vlahovic[a]
[a] Physics Department, North Carolina Central University, Durham, NC, USA [b] Center for Advanced Materials and Smart Structures, North Carolina A&T University, Greensboro, NC, USA

To cite this Article Filikhin, I. , Deyneka, E. , Melikyan, H. and Vlahovic, B.(2005) 'Electron states of semiconductor quantum ring with geometry and size variations', Molecular Simulation, 31: 11, 779 — 785
To link to this Article: DOI: 10.1080/08927020500269445
URL: http://dx.doi.org/10.1080/08927020500269445

Molecular Simulation, Vol. 31, No. 11, 15 September 2005, 779–785

Taylor & Francis
Taylor & Francis Group

Electron states of semiconductor quantum ring with geometry and size variations

I. FILIKHIN*†, E. DEYNEKA‡, H. MELIKYAN† and B. VLAHOVIC†

†Physics Department, North Carolina Central University, 1801 Fayetteville Street, Durham, NC 27707, USA
‡Center for Advanced Materials and Smart Structures, North Carolina A&T University, 1601 E. Market Street, Greensboro, NC 27411 USA

(Received June 2005; in final form July 2005)

Heterostructured semiconductor quantum rings (QR) are studied by a three-dimensional model in a single sub-band approach with energy dependent electron effective mass. Nonlinear confinement energy problem is numerically solved by the finite element method. Effects of boundary conditions corresponding to various QR/substrate configurations are analyzed. General relation for the size dependence of the QR confined energy is derived. The contribution to confinement energy due to the presence of external magnetic field is compared with the effect of variation of QR geometrical parameters. Applicability of the model is tested by comparison with experimental data.

Keywords: Nanoscale materials and structures; Electron states in nanoscale systems; Single particle states; Quantum rings

1. Introduction

Recent successful fabrication of the self-assembled heterostructured quantum dots (QD) and quantum rings (QR) with controlled topology and geometrical properties [1,2] have demonstrated that these structures have significant perspectives for practical photonic device applications. It has also stimulated further theoretical and computational studies with realistic modeling conditions [3–6]. Traditionally applied in the macroscopic scale studies parabolic electron spectrum needs to be replaced by the nonparabolic approach, which is more appropriate to nanoscopic quantum objects [7,8]. In the present paper a model of QR with the energy dispersion defined by the Kane formula (non-parabolic approximation) [9] is employed, and the kp-perturbation theory in a single sub-band approach is applied. This model leads to the confinement energy problem with non-linear Schrödinger equation in 3D space. We have numerically solved this problem using the finite element method (FEM). The effect of QR geometry on the electron states of QR was studied and the magnitude of non-parabolic contribution to the electron confinement energy estimated. Size dependence of the electron energy of QR and QD was subject of several theoretical studies [3,4]. In presented paper, unlike the prior reports, a general relation for the size dependence of the QR energy is derived. This relation was tested for various boundary conditions and combinations of QR/substrate materials. We also compared relative contributions to QR confined energy due to the external magnetic field and QR geometrical size variations. Experiential data obtained in the capacitance–gate voltage measurements are explained within framework of the model.

2. Model description

Semiconductor quantum ring located on the substrate is considered. Geometrical parameters of the QR are the height H, radial width ΔR and inner radius R_1. It is assumed that $H/\Delta R < 1$ (wide ring). QR cross section is schematically shown in figure 1. The discontinuity of conduction band edge of the QR and the substrate forms a band gap potential, which induces confinement electron states. This 3D heterogeneous structure is modeled by employing the kp-perturbation single sub-band approach [10] with energy dependent quasi-particle

*Corresponding author. E-mail: ifilikhin@nccu.edu

Molecular Simulation
ISSN 0892-7022 print/ISSN 1029-0435 online © 2005 Taylor & Francis
http://www.tandf.co.uk/journals
DOI: 10.1080/08927020500269445

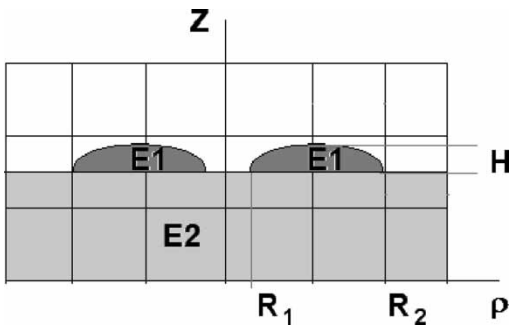

Figure 1. Cross section of the quantum ring (E1) and the substrate (E2). QR geometrical parameters are: H—height, R_1—inner radius, R_2—outer radius.

effective mass. The energies and wave functions of a single electron in a semiconductor structure are the solutions of the Schrödinger equation:

$$(H_{\rm kp}(m^*) + V_c(\mathbf{r}) - E)\Psi(\mathbf{r}) = 0, \qquad (1)$$

where $H_{\rm kp}(m^*) = \mathbf{p}(1/2m^*)\mathbf{p}$ is a single band kp-Hamiltonian operator, m^* is the electron effective mass dependent on the energy E and the position vector $\mathbf{r}$. $V_c(\mathbf{r})$ is the band gap potential, which is equal to zero in QR, and is equal to E_c outside of QR: $V_c(\mathbf{r}) = E_c$, $\mathbf{r} \in$ E1. The value E_c is proportional to the energy misalignment of the conduction band edges of QR (E_g^{QR}) and substrate ($E_g^{\rm S}$) : $E_c = 0.7(E_g^{\rm S} - E_g^{\rm QR})$. Spatial dependence of the electron effective mass is given as $m_i^*(E, \mathbf{r})$, $i = 1,2$, where m_1^* and m_2^* are the masses inside the QR ($\mathbf{r} \in$ E1) and the substrate ($\mathbf{r} \in$ E2), respectively. Within subdomains E1, E2 m_i^* is independent on the coordinates. Taking the limits of spatial influence of the QR confinement state on the substrate into consideration, the range of region E2 is not exactly defined, but rather depends upon confinement energy. This aspect of the presented model was discussed in details in [6].

Energy dependence of the electron effective mass is defined by the Kane formula [9] (non-parabolic approximation):

$$\frac{m_0}{m^*} = \frac{2m_0P^2}{3\hbar^2}\left(\frac{2}{E_g + E} + \frac{1}{E_g + \Delta + E}\right). \qquad (2)$$

Here m_0 is free electron mass, P is Kane's momentum matrix element, E_g is the band gap, and Δ is the spin-orbit splitting of the valence band. Inside the QR, E is the ground state confinement energy. In order to account for the effect of non-parabolicity in the substrate, E should be replaced by $E - E_c$.

3. Method

The non-linear Schrödinger equation (1) is solved by means of the iterative procedure:

$$H_{\rm kp}(m_i^{*,n-1})\Psi^n = E^n\Psi^n, \quad m_i^{*,n} = f_i(E^n), \qquad (3)$$

where n is the iteration number, $i = 1,2$ refers to the subdomains of the system ($i = 1$ for the QR (E1), and $i = 2$ for the substrate (E2)), f_i is the function defined by equation (2). The initial values $m_i^{*,0}$ are equal to the bulk values of the corresponding materials. For each iteration the problem (1) is reduced to a solution of the Schrödinger equation. Considering axial symmetry of the QR, this equation may be written in the cylindrical coordinates (ρ, z, ϕ):

$$\left(-\frac{\hbar^2}{2m^*}\left(\frac{\partial^2}{\partial\rho^2} + \frac{1}{\rho}\frac{\partial}{\partial\rho} - \frac{l^2}{\rho^2}\right) - \frac{\hbar^2}{2m^*}\frac{\partial^2}{\partial z^2} + V(\rho,z)\right)\Phi(\rho,z) = -E\Phi(\rho,z). \qquad (4)$$

The wave function can be written as: $\Psi(\mathbf{r}) = \Phi(\rho, z)\exp(il\phi)$, where $l = 0, \pm1, \pm2, \ldots$ is the electron orbital quantum number. The ground state is defined as the state with minimal energy. Boundary conditions for this QR/Substrate configuration are: $\Phi(\rho, z) \to 0$ when $(\rho, z) \to \infty$, where $(\rho, z) \in$ substrate and $\Phi(\rho, z) = 0$ on the upper surface of QR and the substrate. It is assumed that the wave function $\Phi(\rho, z)$ and the first order derivative of the form $(\hbar^2/2m^*)(\mathbf{n}, \nabla)\Phi$ are continuous throughout the subdomain interfaces E1, E2 and E3 (see figure (1)). The equation (4) was solved by FEM utilizing FEMLAB[†]. Spatial domain of the solution was meshed with consecutive decrease of the mesh size to determine optimal mesh. Then the iterative procedure (3) was applied. This procedure usually required 3–6 iterations to achieve convergence with relative accuracy of 10^{-2} for the effective mass.

4. Effect of size variation

The effect of QR geometry on the electron ground states was studied through variations of the height H, radial width ΔR and inner radius R_1. Calculated electron ground state energies as functions of ΔR (a) and H (b) are shown in figure 2. Similar dependencies were obtained earlier [3,4]. It is worth noting, that the electron ground state of QR in zero magnetic field is practically independent on the inner radius R_1 (3–24 nm). This result agrees with calculations of [4].

It is evident from our calculations that there is a significant difference between the non-parabolic and parabolic approximations. The results of calculations with parabolic approximation are shown in figure 2 by dashed lines. Relative difference between the confinement energies calculated in parabolic and non-parabolic approximations is shown in figure 3. One can conclude that contribution of the non-parabolic effect increases rapidly with QR size decreasing.

General relation for the size dependence of the QR confinement energy has been obtained. As follows from

[†]www.comsol.com

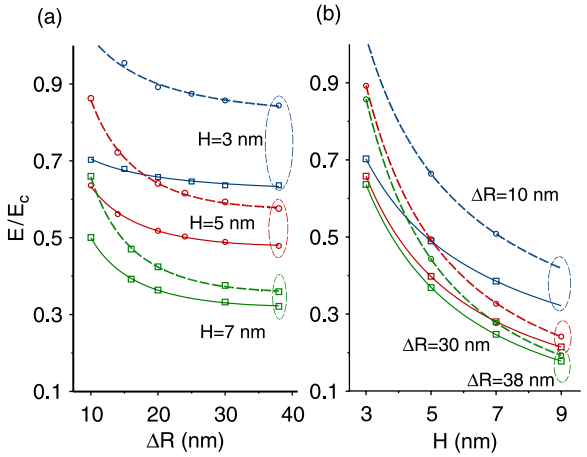

Figure 2. Electron ground state energy of InAs/GaAs QR with non-parabolic (dashed line) and parabolic (solid lines) approximation as functions of (a) QR width ΔR at varied height H, (b) QR height H at varied radial width ΔR. Inner radius R_1 is 17 nm, $E_c = 0.77$ eV.

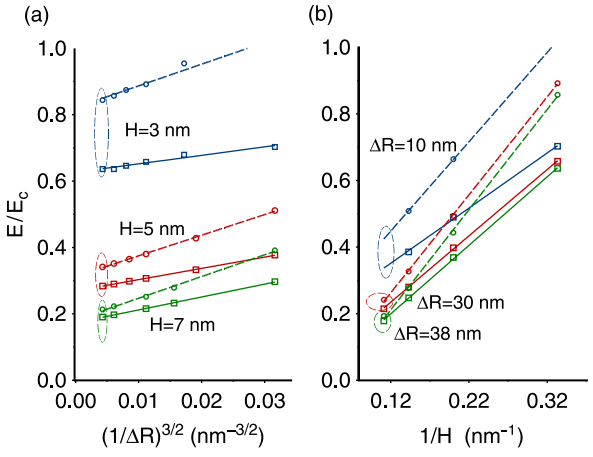

Figure 4. Electron ground state energy of InAs/GaAs QR as function of (a) $(1/\Delta R)^{3/2}$ for various height H, (b) $1/H$ for various radial width ΔR. All notations are as in figure 2.

our analysis, the ground state energy of QR can be best described mathematically by the power function of the inverse height and radial width:

$$E \approx a\left(\frac{1}{\Delta R}\right)^{\gamma} + b\left(\frac{1}{H}\right)^{\beta}, \qquad (5)$$

where a and b are constants. Within framework of the considered model the values of the power coefficients $\gamma = 3/2$ and $\beta = 1$ were obtained numerically by the least square method. It is showed in figure 4 where one can see that the graphs $E = E(\Delta R^{-\gamma})$ and $E = E(H^{-\beta})$ become linear with a good degree of accuracy. This general result relates to typical experimental values of the QR geometry: $1 < H < 8$ nm, and $3 < \Delta R < 50$ nm [1]. The relation (5) was tested in the following two case studies. The first case included modeling of different QR/Substrate material combinations. We have considered InAs/GaAs, Ge/Si, CdTe/CdS heterostructures, which are often used for QR and QD manufacturing [1].

Experimental values of the parameters of QR and substrate materials [11] are given in table 1. In figure 5 the ground state energy as a function of $(1/\Delta R)^{3/2}$ is depicted for chosen QR/Substrate structures. One can see that this dependence is holding true for all three material combinations. From figure 5 one can also notice that observed non-parabolic effect is significant when the size parameters of QR are within the following range: for InAs/GaAs: $H < 7$ nm, $\Delta R < 30$ nm; for Ge/Si: $H < 5$ nm, $\Delta R < 20$ nm; for CdTe/CdS $H < 4$ nm, $\Delta R < 15$ nm. The constants a and b had to be adjusted for each considered combination of materials.

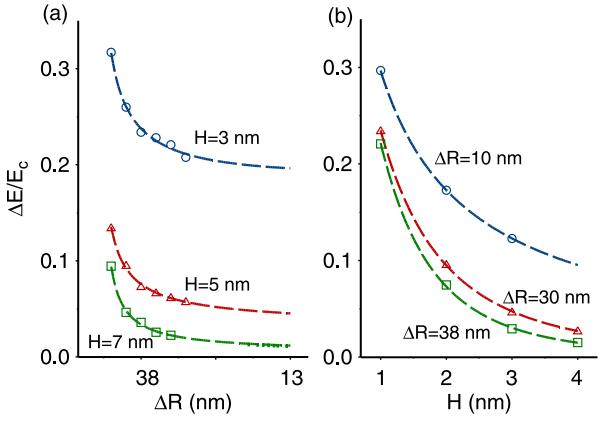

Figure 3. Non-parabolic contribution $\Delta E/E_c$ into the electron confinement energy of the InAs/GaAs QR at different geometrical parameters. All notations are as in figure 2.

The second case was related to modeling of the boundary conditions. Three boundary conditions models were considered, each corresponding to a different physical situation. The first is a model of isolated QR, or the "infinity wall" model. The second one is the model considered above (see figure 1) which we describe as "one side wall" model. The third is the model considered in [4,5], which can be called "no infinity wall". That model represents the situation when the QR is embedded into the substrate. Figure 6 shows the cross sections of QR/substrate configuration for the each boundary conditions model. It was found that the change in boundary conditions of the problem (4) leads to a change of value of the power coefficients in (5). In figure 6 the power coefficients for each boundary conditions model are listed. It is not surprising that for the "infinity wall" model these coefficients are equal to 2. For this model the analytical solution of (4) is possible by the separation of variables ρ and z and reducing to one-dimension problem for the potential well with the infinity wall [12].

Calculated confinement energy of QR is changing when the model of figure 6c is transformed to the model of figure 6b. This geometrical effect is illustrated in figure 7. It shows how the electron energy of QR is changing upon the "immersion" depth D of the QR into the substrate.

Table 1. Parameters of the QR and substrate materials.

QR materials	$m^*_{0,1}/m^*_{0,2}$(*in* m_0 *units*)	E_c, *eV*	$(2m_0P_1^2)/\hbar^2/(2m_0P_2^2)/\hbar^2$	Δ_1/Δ_2
InAs/GaAs	0.024/0.067	0.77	22.4/24.6	0.34/0.49
Ge/Si	0.041/0.200	0.46	16.3/4.0	0.028/0.044
CdTe/CdS	0.11/0.20	0.66	15.8/12.0	0.80/0.07

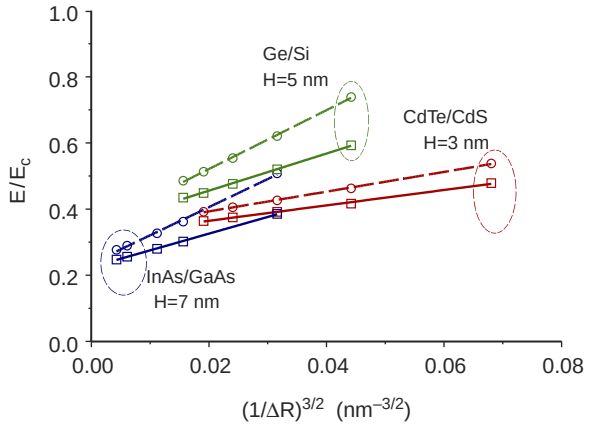

Figure 5. Electron ground state energy of InAs/GaAs QR as function of $(1/\Delta R)^{3/2}$ for various QR/substrate combinations. All notations are as in figure 2.

5. Effect of magnetic field

The idea behind considering the QR confined energy problem in an external magnetic field was to compare relative contributions of the magnetic field and the variations of QR size. The magnetic term, added to the left-hand side of the equation (4), is having the following form:

$$V_m(\rho) = \frac{1}{2m^*}\left(\beta l\hbar + \frac{\beta^2}{4}\rho^2\right),$$

where, $\beta = eB$, B is the strength of the magnetic field, normal to the plane of QR. The spin of electron is not taken into the account in this model, because experimentally observed Zeeman spin-splitting is relatively small [13]. In magnetic field there is a manifestation of Aharonov-Bohm effect [14] on QR electron ground state. Since the ground state energy of QR *Eg.s.* should always have minimal value, the shape of *Eg.s.* in increasing magnetic field represents a series of transitions between successive states with different angular momentum $l = 0, -1, -2, \ldots$ [15].

As it is shown in figure 8 size-dependent energy variations are dominating the effect caused by the magnetic field. One can see that a change in the ground state energy after applying a relatively large magnetic field $B = 8$ T is minimal (~ 3 meV). Even small (4%) variations of QR size can produce the shift of energy levels, exceeding this value (figure 8b and c). At the same time it is known that the size errors during QR fabrication can reach 10% [2]. Apparently, in order to fully utilize the effect of magnetic field on the electron ground state energy, the size precision of manufactured QRs should be improved.

6. Comparison with experiment

To compare the calculations with experimental data, QR geometrical parameters were chosen to be close to that reported for experimentally fabricated QR [1,2]. Our consideration was based on a simple fabrication model, where the initial QD is transformed to QR without the loss of QD material. The volume of obtained QR is equal to the volume of initial QD. Experimentally produced QDs had an average radius of 10 nm and height of 7 nm [1,2]. In our

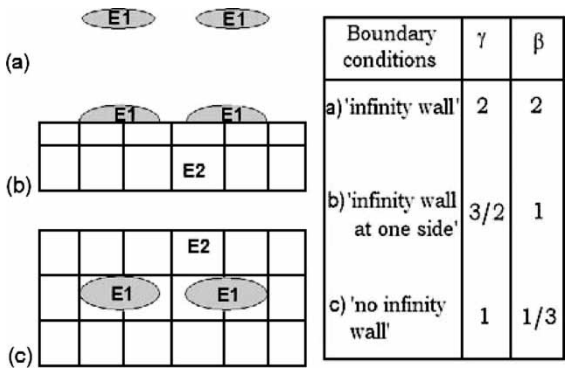

Boundary conditions	γ	β
a) 'infinity wall'	2	2
b) 'infinity wall at one side'	3/2	1
c) 'no infinity wall'	1	1/3

Figure 6. Cross section of the QR/Substrate structure and various models of boundary conditions (left). QR (substrate) are marked as E1 (E2). Boundary condition models and power coefficients in relation (5) (right).

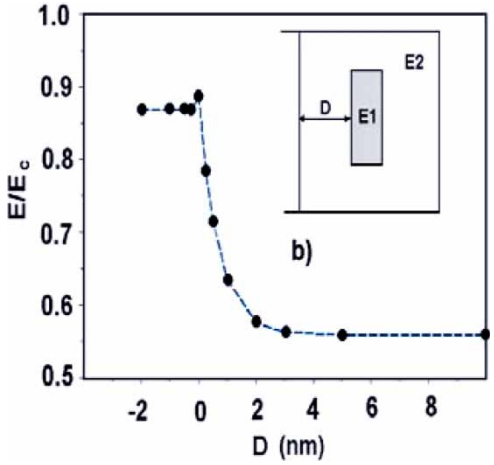

Figure 7. (a) Normalized electron ground state energy of cylindrical shape InAs/GaAs QR as a function of the QR immersion depth D; (b) cross section of QR/substrate structure: $H = 2$ nm, $R_1 = 10$ nm, $\Delta R = 10$ nm.

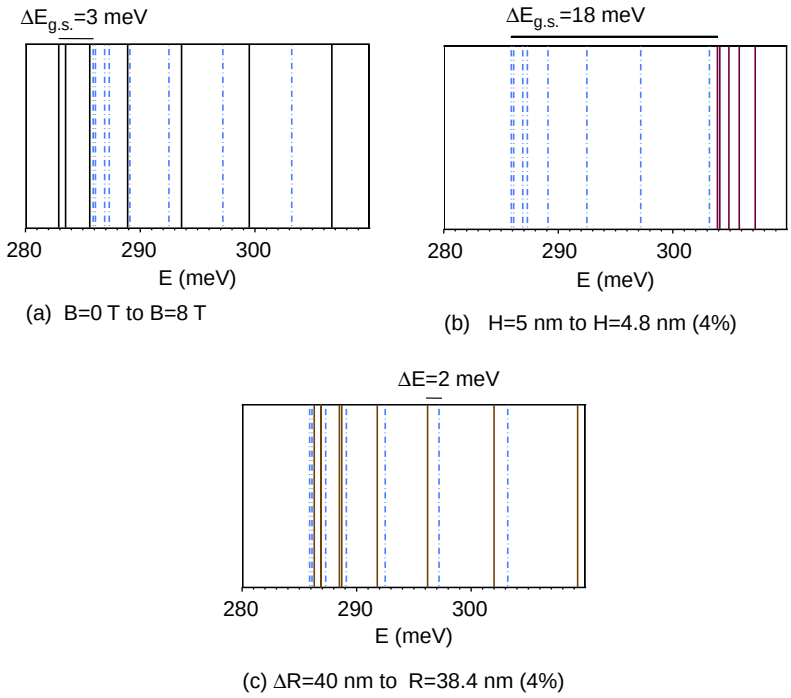

Figure 8. Electron energy spectra of InAs/GaAs QR in magnetic field $B = 8$ T for various size parameters. Numbers on the top of figures refer to the energy levels shift due to the size change, (a) solid lines are the spectrum at $B = 0$, dashed lines—the spectrum at $B = 8$ T, ($\Delta R = 40$ nm, $H = 5$ nm) (b) and (c) dot-dashed lines correspond to the calculation with $\Delta R = 40$ nm, $H = 5$ nm; solid lines—calculations for various QR size parameters: for (b) $\Delta R = 40$ nm, $H = 4.8$ nm; for (c) $\Delta R = 38.4$ nm, $H = 5$ nm.

calculations the inner radius of QR R_1 was set at 10 nm as compared to the radius of initial QD used for the QR production. The height of QR was chosen as $H = 1.3$ nm, and the outer radius R_2-35 nm. Maximal radial thickness of QR was 18 nm [2]. The shapes of QD and QR are shown in figure 9a and b). The results of capacitance-gate-voltage (CV) measurements for QD and QR from [2] are given in figure 10a. The orbital quantum numbers of the states are denoted by upper letters. Observed dual peaks indicate a presence of the electron level splitting due to the Coulomb repulsion [16]. The results of calculations are shown in figure 10a by the arrows. Note that in our model this "Coulomb blockade" [16] effect cannot be taken into the account, therefore the middle values between observed peaks were used to compare calculated and experimental values. Figure 10b represents calculated spectral positions of the low-lying energy levels of QD and QR. To compare the results given in figures 9a and 10a experimentally measured differences in gate-voltage for various electron states were recalculated into the energy of excitation. The voltage to energy conversion coefficient $f = (e\Delta V/\Delta E)$ was defined by the experiment configuration as $f = 7$ [16]. In figure 10a the calculation with this value for f are presented. The ranges of measured energies are marked by gray color stripes in Figure 10b. One can see that the results of calculations qualitatively resemble the experiment. It is important to note here that in prior QR studies [2,17] the value $f = 1.8$ was obtained from comparison of theoretical and experimental data for an addition to the energy of QR ground state in the external magnetic field [2]. This value has been tested within framework of our model. This is shown in figure 11 for the two shapes the QR. Calculations for the QR of figure 9b are shown by open squares, and results for

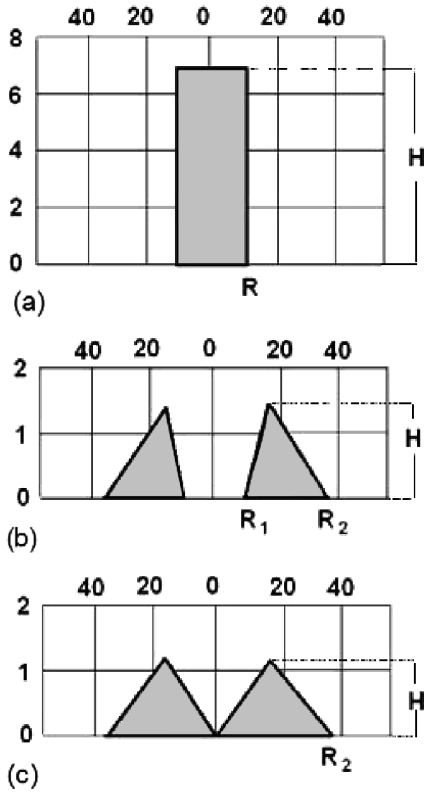

Figure 9. Cross sections of QD (a) and QR (b)–(c).

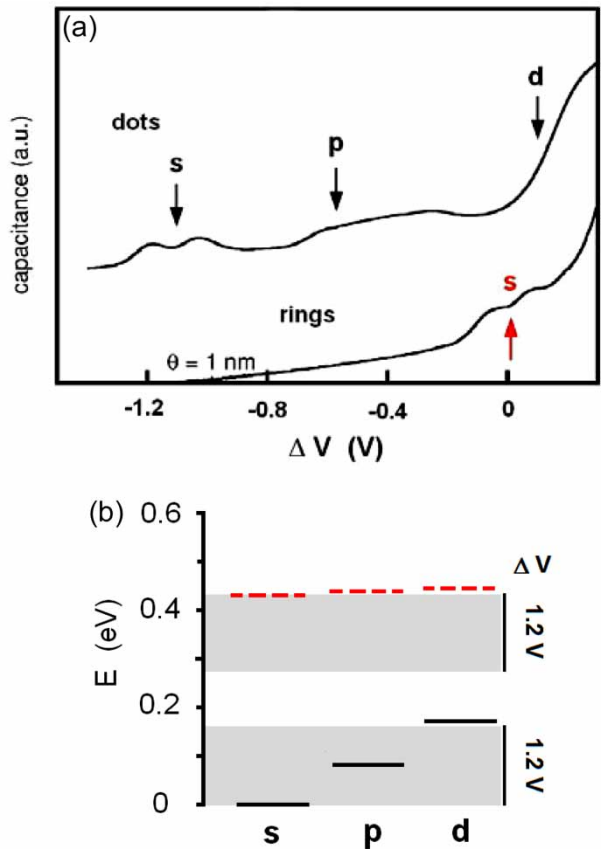

Figure 10. (a) Capacitance gate voltage measurements for QD and QR from [2]. The orbital quantum state is marked by upper letters. Results of calculations are shown by arrows. (b) Calculated spectral positions of the low-lying energy levels ($n = 1$) of QD (solid lines) and QR (dashed lines). The ranges of energies measured in experiments are marked by gray color stripes.

the QR of figure 9c are denoted by open circles. (We still assume that QRs of both shapes have the same volumes.) As it follows from figure 11, our calculations confirm the value of $f = 7$. One can see the effect of Aharonov-Bom-like oscillations for QR ground state energy in magnetic field. This effect is accompanied by a change in the orbital quantum number l of the ground state. It is shown in figure 11 by gray color accentuation of calculation for the QR of the figure 9b shape. Comparison of results for QR of different shapes gives possible explanation for the absence of explicit oscillations in experiential data shown in figure 11. It is clear that even slight shape and size variations of QRs in experimentally produced QR arrays [2] can lead to leveling of the oscillations.

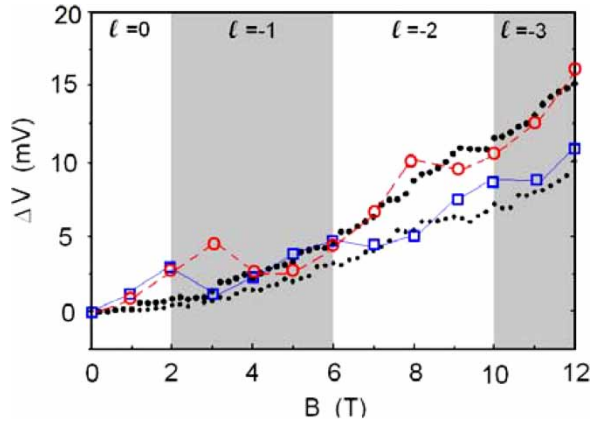

Figure 11. Addition to the electron ground state energy of QR in external magnetic field B. Experimental data are shown by solid circles. Small circles correspond to the case when a single electron is in QR; large circles is the observed data for two electrons in QR. Calculated energies are marked by open squares (model (b) from Figure 9 and open circles model (c) from Figure 9).

7. Summary

Semiconductor quantum ring has been studied in the single sub-band approach with energy dependence of the electron effective mass. Realistic boundary conditions corresponding to various experimental QR/substrate configurations and the effects of non-parabolicity of the electron spectra of the carriers were accurately considered. It is shown that main size factors defining the electron confinement state of QR are the height H and the radial width ΔR. Functional form of relation between the ground state energy end geometrical parameters of QR was derived for different QR/substrate designs. It is shown that the size and form factors can be dominant in experimentally interesting studies of QR in the external magnetic field. It was concluded that presented model is applicable for adequate description of the experimental data.

Acknowledgements

This project is supported by the Department of Defense through grant No. DAAD 19-01-1-0795. I.F. is also partially supported by NASA grant NAG3-804.

References

[1] J.M. Garsia, G. Medeiros-Ribeiro, K. Schmidt, T. Ngo, J.L. Feng, A. Lorke, J.P. Kotthaus, P.M. Petroff. Intermixing and shape changes during the formation of InAs self-assembled quantum dots. *Appl. Phys. Lett.*, **71**, 2014 (1997).
[2] A. Lorke, R.J. Luyken, A.O. Govorov, J.P. Kotthaus, J.M. Garcia, P.M. Petroff. Spectroscopy of nanoscopic semiconductor rings. *Phys. Rev. Lett.*, **84**, 2223 (2000).
[3] S.S. Li, J.B. Xia. Electronic states of InAs/GaAs quantum ring. *J. Appl. Phys.*, **89**, 3434 (2001).
[4] Y. Li, O. Voskoboynikov, C.P. Lee. Computer simulation of electron energy states for three-dememsional InAs/GaAs semicondactor quantum ring. *Proceedings of the International Conference on Modeling and Simulating of Microsystems (San Juan, Puerto Rico, USA)*, p. 543, Computational Publication, Cambridge (2002).
[5] O. Voskoboynikov, C.P. Lee. Magnetzation and magnetic susceptibily of InAs nano-ring. *Physica E*, **20**, 278 (2004).
[6] I. Filikhin, E. Deyneka, B. Vlahovic. Energy dependent effective mass model of InAs/GaAs quantum ring. *Modelling Simul. Mater. Sci. Eng.*, **12**, 1121 (2004).
[7] C. Wetzel, et al. Electron effective mass and nonparabolicity in Ga0.47In0.53As/InP quantum wells. *Phys. Rev. B*, **53**, 1038 (1996).
[8] H. Fu, L.-W. Wang, A. Zunger. Applicability of the k.p method to the electronic structure of quantum dots. *Phys. Rev. B*, **57**, 9971 (1998).

[9] E. Kane. Band structure of indium antimonide. *J. Phys. Chem. Solids*, **1**, 249 (1957).
[10] J.M. Luttinger, W. Kohn. Motion of electrons and holes in perturbed periodic fields. *Phys. Rev.*, **97**, 869 (1955).
[11] M. Levinshtein, S. Rumyantsev, M. Shur. *Handbook Series on Semiconductor Parameters*, World Scientific, Singapore (1999).
[12] L.D. Landau, E.M. Lifschitz. *Quantum Mechanics*, Pergamon Press, Oxford (1977).
[13] G. Medeiros-Ribeiro, M.V.B. Pinheiro, V.L. Pimentel, E. Marega. Spin splitting of the electron ground states of InAs quantum dots. *Appl. Phys. Lett.*, **80**, 4229 (2002).
[14] Y. Aharonov, D. Bohm. Significance of electromagnetic potential in the quantum theory. *Phys. Rev.*, **115**, 485 (1959).
[15] N. Kim, G. Ihm. Electronic structure of a magnetic quantum ring. *Phys. Rev. B*, **60**, 8767 (1999).
[16] B.T. Miller, W. Hansen, S. Manus, R.J. Luyken, A. Lorke, J.P. Kotthaus, S. Huant, G. Medeiros-Ribeiro, P.M. Petroff. Few-electron ground states of charge-tunable self-assembled quantum dots. *Phys. Rev. B*, **56**, 6764 (1997).
[17] A. Emperador, M. Pi, M. Barranko, A. Lorke. Far-infrared spectroscopy of nanoscopic InAs rings. *Phys. Rev. B.*, **62**, 4573 (2000).